Ocean and Coastal Management 254 (2024) 107193

Contents lists available at ScienceDirect

Ocean and Coastal Management

journal homepage: www.elsevier.com/locate/ocecoaman

Analysis of the coastal flooding exposure of embayed beaches at a regional scale using a video monitoring network: Basque Coast (Spain)

Aritz Abalia [a,b,*], Iñaki de Santiago [a], Pedro Liria [a], Roland Garnier [a], Irati Epelde [a], Asier Nieto [a], Denis Morichon [b]

[a] AZTI Marine Research, Basque Research and Technology Alliance (BRTA), Herrera Kaia. Portualdea z/g, 20110, Pasaia, Gipuzkoa, Spain
[b] Université de Pau et des Pays de L'Adour, UPPA, SIAME, Anglet, 64600, France

ARTICLE INFO

Keywords:
Coastal videometry network
Storm impact
Geomorphology
Nearshore hydrodynamics
Regional scale
Coastal management strategies
Decision support tool

ABSTRACT

Coastal zones are highly exposed to storm waves that can affect natural values and damage coastal facilities and engineering structures to varying degrees. The definition of a regional management strategy along the Basque Coast (150 km), composed mainly of embayed beaches, is challenging due to the high variability in the coastal flooding exposure, nearshore wave conditions and geomorphological characteristics. Here, 3 years of data (2019–2022) from a coastal video-monitoring network (KOSTASystem) deployed at 13 beaches were used to: i) assess the regional variability of storm impact associated to coastal flooding (hereinafter referred as storm impact), ii) analyse the relation between storm impact, nearshore hydrodynamics and pre-storm geomorphology and iii) find common beach behaviours, using an extensive video monitoring network operating along the Basque Coast on a series of embayed beaches. Different types of images were analysed during storms to characterise storm impact through the storm impact regime indicator (SIR, *i.e.* swash/collision/overtopping). The storm impact was compared against nearshore hydrodynamics (water level and energy flux) and geomorphological parameters, (1) the dry beach width (DBW) obtained from orthorectified Timex images in a predefined profile and (2) the dune/seawall toe (TH) and (3) crest (CH) height obtained from airborne LiDAR (Light Detection and Ranging) surveys. No clear relation was found between nearshore wave conditions and storm impacts. This might be related to the reduced range in the wave and tide values used to perform the analysis during high energy conditions. However, beaches with a wider dry beach and/or higher dune/seawall toe and crest lead to lower storm impact intensity (swash) and inversely (collision/overtopping). The beaches of the study site were described in function of the storm impact regime and the pre-storm geomorphological parameters (heights referred to the 0 of the Spanish topographic institute (NMMA IGN 2008)) as: Group 1) Beaches dominated by the collision regime that present low values of DBW and TH, specifically, DBW < 30 m and TH < 3.5 m. Group 2) Beaches dominated by the swash with few collision events that present moderate DBW and relatively high values of TH, specifically, 40 < DBW < 75 m and 4 < TH < 6.5 m. Group 3) Beaches fully dominated by the swash regime that present relatively high values of DBW and TH, specifically, DBW > 50 m and 4 < TH < 7.5 m. This coastal exposure assessment at regional scale benefits stakeholders and coastal managers by characterising the most exposed areas and identifying the drivers. The results presented here are expected to be valid in sites with similar wave climate and water level regimes. The application of the methodology to other coastal areas with a regional videometry network would help to generalize and give robustness of the results.

1. Introduction

Embayed beaches form half of the world's coastline (Daly et al., 2011). As their location is apparently protected, they are usually characterised by a high degree of urbanisation and represent a key zone for human development. However, those areas, like most coastal regions, are exposed to storm waves that can affect natural values and damage coastal facilities and engineering structures to varying degrees. Consequently, a coastal region dominated by embayed beaches can be moderately to highly exposed to storm impact. In this context, the

* Corresponding author at: AZTI Marine Research, Basque Research and Technology Alliance (BRTA), Herrera Kaia. Portualdea z/g, 20110, Pasaia, Gipuzkoa, Spain.
E-mail address: aabalia@azti.es (A. Abalia).

https://doi.org/10.1016/j.ocecoaman.2024.107193
Received 15 July 2023; Received in revised form 26 April 2024; Accepted 14 May 2024
Available online 21 May 2024

coastal hazards management and decision-making processes have to be taken at a regional level (Toimil et al., 2023). This implies that coastal managers need a better characterisation and understanding of the impacts of storms to support regional coastal management strategies and identify the most exposed beaches that would require special attention and in some cases priority investment.

The development of coastal management strategies at a regional scale would benefit from data with high spatial and temporal resolution covering simultaneously storm impacts and geomorphological characteristics. Storm impact can be represented by different indicators, either related to beach erosion, such as, dune or shoreline erosion or coastal flooding, such as, overtopping discharge, flood extension or the well-known and widely-applied storm impact scale (Sallenger, 2000). There are studies conducting in situ field surveys to address beach erosion indicators during storms at local scale (Cohn et al., 2022; Splinter et al., 2018b), however, none of them address coastal flooding indicators due to the difficulties associated with their measurement, for instance, safety risks, limited accessibility and resource constraints. Indeed, studies conduct numerical simulations to assess coastal flooding storm impacts at local scale through numerical models (de Santiago et al., 2018; Morichon et al., 2018; Cueto Fonseca et al., 2021; Mucerino et al., 2019), empirical formulations (Stockdon et al., 2007; Silveira et al., 2016; Almeida et al., 2012; Vousdoukas et al., 2012) and Bayesian Networks (Callens et al., 2022) calibrated with in situ measurements. The application at a regional scale of the results provided by the above-mentioned studies is challenging as they usually depend on specific wave climate conditions and geomorphological characteristics. Stokes et al. (2021) developed a forecasting system including the description of wave transformation processes such as shoaling, breaking, runup and overtopping through empirical equations to predict and assess the wave overtopping and the associated hazard level over the entire 1000 km coastline of southwest England. The proposed system predicted the overtopping with accuracy and differentiates hazard events. Medellín et al. (2021) studied the effect of Climate Change to storm impacts at four beaches along the northern Yucatan coast using the numerical nearshore wave model SWASH (Zijlema et al., 2011) with default calibration parameters. This numerical study shows that subtidal parameters such as beach slope and sandbars, and subaerial parameters including berm and dune elevations play an important role on the intensity of storm impact. More recently, Toimil et al. (2023) studied the influence of coupling coastal flood projections and beach erosion for different climate change scenarios along a 40-km coastal stretch in the Spanish Mediterranean. Total water levels were computed through the calibrated XBeach model (Roelvink et al., 2009) highlighting storm erosion and profile geometry as the most influential factors. While the previous studies demonstrated the potential of current numerical tools to provide new knowledge to assist coastal management strategies at a regional scale, they require to carry out simultaneous field campaigns for model calibration and validation at several sites over large period of time, what could be prohibiting when dealing with a large stretch of coastline.

Videometry is used worldwide since it provides several advantages as a remote monitoring technique. Indeed, it allows to monitor coastal processes over a large range of temporal and spatial scales (Splinter et al., 2018a; Andriolo et al., 2019; Santos et al., 2020; Liria et al., 2021; Epelde et al., 2021; Addona et al., 2022). It is generally used at local scale to study coastal stability problems on sandy coastlines (Kroon et al., 2007) looking for instance to dynamic changes of nearshore morphology based on long-term (Splinter et al., 2018a) and short-term (Andriolo et al., 2019; Santos et al., 2020) video image datasets. It can also be used for the characterisation of storm impacts related to coastal flooding for numerical model calibration and validation purposes (de Santiago et al., 2017, 2018; Morichon et al., 2018; Callens et al., 2021; Mucerino et al., 2019; Stokes et al., 2021; Silveira et al., 2016). The main hypothesis of the present work is that a series of video stations can be deployed simultaneously at several sites during a large period of time allowing to carry out comparative analysis and define indicators that can help to understand the beach behaviour.

The present study aims to: i) assess the regional variability of storm impact associated to coastal flooding (hereinafter referred as storm impact), ii) analyse the relation between storm impact, nearshore hydrodynamics and pre-storm geomorphological parameters and iii) find common beach behaviours, using an extensive video monitoring network operating along the Basque Coast on a series of embayed beaches. The Basque Coast (northern Spain) is a study site of strong interest since it is representative of a highly exposed coastal area to storms (Liria et al., 2011), which has been monitored for several years (Liria et al., 2021; de Santiago et al., 2013, 2017, 2018, 2021; Epelde et al., 2021; Chust et al., 2022). This study shows that the knowledge integration, based on the combination of two different knowledge structures, nearshore dynamics and video-monitoring techniques, into a single structure, can provide valuable information and guidelines to support coastal management strategies at regional scale. It will also demonstrate the interest to maintain a regional and temporally permanent videometry network that can help to support regional management strategies.

The study area, the videometry network and the offshore hydrodynamic forcings are described in Section 2. This section outlines the geomorphological components of each site, the characteristics, configuration and available data of the corresponding videometry station. Furthermore, it presents the procedure used to identify storms that occurred during the study period. Section 3 is focused on the wave propagation procedure used to obtain the nearshore wave conditions at each site. It also describes the method used to determine the storm impact intensity and the pre-storm geomorphological parameters using videometry images. The assessment of the storm impact variability, the identification of the drivers that influence the intensity of the impact and the determination of common beach behaviours are studied in Section 4. Finally, the advantages, disadvantages and good practises for stakeholders related to the use of videometry networks, the influence of hydrodynamic and pre-storm geomorphological parameters in the storm impact and the recommendations for further research and application for coastal management are discussed in Section 5.

2. Study area and datasets

2.1. Study area

The Basque Coast (northern Spain) presents a great variety of embayed beaches located in highly urbanised and natural environments (de Santiago et al., 2021). The length of the coastline is approximately 150 km. For the present study, 13 embayed beaches belonging to the AZTI's Basque Coast monitoring network (Fig. 1) were selected.

Along the study area, the grain size ranges from 0.25 to 0.5 mm (Table 1). There are 9 west-facing beaches and 4 east-facing beaches, covering angles between WNW and ESE clockwise (Table 1). The embayment degree, estimated according to the classification of Fellowes et al. (2019) varies between 0.55 (lower degree of embaymentisation, class 1) and 1.32 (high degree of embaymentisation, class 3) and also includes intermediate values (medium degree of embaymentisation, class 2) (Table 1).

The offshore wave climate is dominated by a mean significant wave height (H_s) of 1.5 m, a peak period (T_p) of 10 s and a main direction (Dir) of 350° (de Santiago et al., 2021). The wave energy is seasonally variable, being winters (Dec-Mar) and summers (Jun-Sep) the most and less energetic seasons, respectively (González et al., 2004). The tidal regime is semi-diurnal, with a mean (maximum) annual tidal range around 3 m (4.5 m). At spring (neap) tides, it is defined as high-mesotidal (low-mesotidal) (González et al., 2004). The storm surge can vary between −0.5 m and 1 m in the study area (de Santiago et al., 2021).

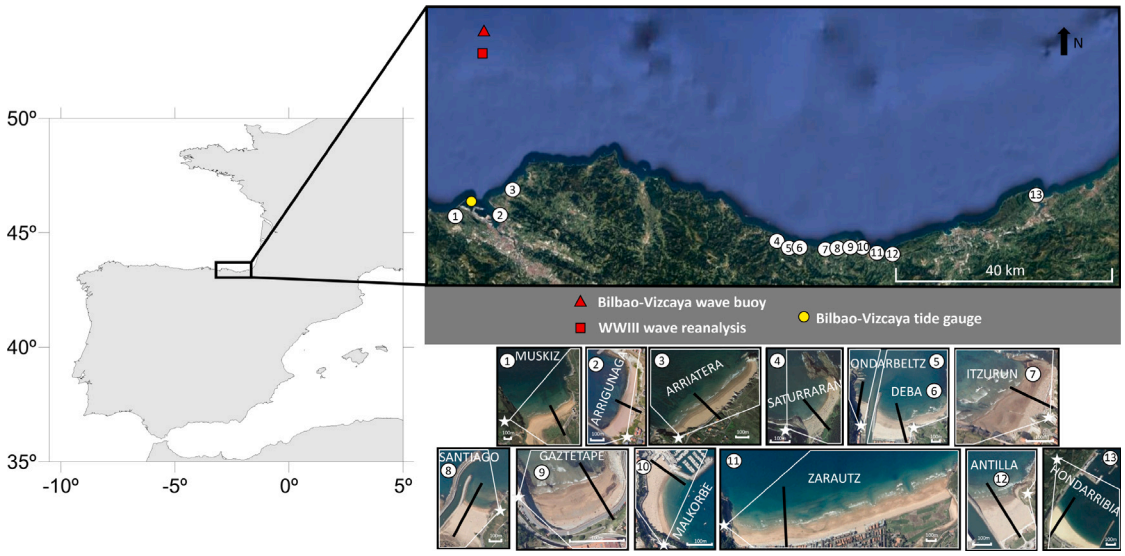

Fig. 1. The Basque Coast (northern Spain). Location of beaches under study, from west to east, Muskiz, Arrigunaga, Arriatera, Saturraran, Ondarbeltz, Deba, Itzurun, Santiago, Gaztetape, Malkorbe, Zarautz, Antilla and Hondarribia. Red triangle: Bilbao-Vizcaya wave buoy. Red square: Wavewatch III wave reanalysis. Yellow circle: Bilbao 3 tidal gauge. Dark line: analysed profiles in each beach. White stars: approximated location of videometry stations. White polygons: area captured by the videometry stations.

Table 1
Study area. Mean grain size (D_{50}), orientation and embayment degree for the 13 studied beaches. The numbers (N°) refer to the beaches shown in Fig. 1.

N°	Beach	D50 (mm)	Orientation	Embayment degree
1	Muskiz	0.31	N30W	0.82
2	Arrigunaga	0.46	N60W	0.85
3	Arriatera	0.32	N45W	0.55
4	Saturraran	0.50	N60W	0.89
5	Ondarbeltz	0.31	N10E	1.31
6	Deba	0.25	N10W	0.83
7	Itzurun	0.31	N70W	1.07
8	Santiago	0.33	N25E	1.32
9	Gaztetape	0.34	N20W	1.06
10	Malkorbe	0.26	S65E	0.97
11	Zarautz	0.31	N15W	0.48
12	Antilla	0.42	N30W	1.26
13	Hondarribia	0.27	N30E	1.22

2.2. Videometry network

Coastal video monitoring provides high-frequency, high-quality and continuous images of the nearshore area. This remote sensing technique allows the monitoring of the dynamic changes of the coastal zone and the characterisation of storm impacts. The KOSTASystem technology, used in this study, was launched in 2007 and is currently implemented in 20 operational stations that forms the Basque videometry network (Liria et al., 2021; Epelde et al., 2021). Due to the relatively short historical data recorded by the recently installed stations (7 videometry stations set-up during 2020) 13 videometry stations are used in the present work (Table 2). The overlapping period between these 13 stations extends between April of 2019 and April of 2022, hourly, corresponding to the study period. There are two types of stations in the Basque videometry network; autonomous stations, which are equipped with photovoltaic panels and non-autonomous stations, which are connected to the electrical grid. Autonomous stations capture hourly images between 8 am and 4 pm (UTC) while non-autonomous stations capture images every 30 min between 7 am and 5 pm (UTC), with the exception of the station of Zarautz, which includes a NIR (Near-Infrared) camera that is operational 24 h and therefore, not restricted to daylight hours as the other stations. The used products in the KOSTASystem technology are derived from the temporal processing of images based on the open-source SIRENA software (Nieto et al., 2010; Liria et al., 2021). The technology creates four different types of images: Snap (instantaneous images), Timex (captured images averaged every second for 10 min), VAR (variance images) and Timestack (images representing time-varying pixel intensities along a given transect across the shoreline in the camera field of view). Then, camera calibration and orthorectification routines are based on Holland et al. (1997). This methodology consists in the calibration of the intrinsic and extrinsic parameters of the camera and allows to extract measurable information from the images on a uniform z plane or over a predefined digital terrain model grid. The cameras spatial resolution varies between 0.1 and 0.4 m and between 1 and 7 m in the cross-shore and alongshore directions respectively. Since these systems are exposed to adverse weather conditions (rain, salt spray, wind), connection and/or image quality problems may occur (camera malfunctions), resulting in loss of data. During the daylight hours of the study period, the number of available (loss) Snap and Timex images (based on the percentages represented in Table 2) ranges between 11 500 (6000) and 17 000 (500) along different stations. The Timestack image percentage data is generally lower and in some cases zero due to erroneous commissioning of the system.

2.3. Wave and tide data

2.3.1. Data sources

Offshore wave conditions during the study period were measured by the Bilbao-Vizcaya wave buoy (Fig. 1) operated by Puertos del Estado (http://www.puertos.es) since 1990. In order to extend the database and complete some gaps, a hindcast data base computed with Wavewatch III (WW3 v5.16, Tolman (2016)) by the SHOM (https://data-dataref.ifremer.fr/ww3-hycom-era5/) was used spanning from 1979 to 2022. The tidal data is provided by the Bilbao 3 tidal gauge (Fig. 1) operated by Puertos del Estado (http://www.puertos.es) since 1992. The data reference is the 0 of the Spanish topographic institute (NMMA IGN 2008) and therefore translated from the mean sea level (+0.34 m).

2.3.2. Energetic events

The characterisation of energetic events requires to select threshold values that allow to separate ordinary wave conditions from significantly energetic conditions. In the present study, energetic events are defined when the H_s value exceeds the H_{s90} (3.7 m) coinciding with

Table 2
Characteristics of videometry stations. The numbers (N°) refer to the beaches shown in Fig. 1.

N°	Beach	Station height (m)	Configuration	Number of cameras	Acquisition interval (minutes)	Available data (since)	Available data (light hours)		
							Snap	Timex	Timestack
1	Muskiz	39.7	Non-autonomous	5	30	April 2012	97.1	97.1	74.3
2	Arrigunaga	47.9	Non-autonomous	2	30	November 2017	85.2	85.2	85.2
3	Arriatera	43.5	Non-autonomous	2	30	January 2018	74.7	74.7	60
4	Saturraran	49.9	Autonomous	2	60	February 2019	69.6	69.6	64.1
5	Ondarbeltz	10	Autonomous	2	60	April 2019	78.4	78.4	0
6	Deba	16.5	Non-autonomous	4	30	July 2018	78.6	78.6	78.3
7	Itzurun	20.9	Autonomous	2	60	April 2019	70.9	70.9	28.2
8	Santiago	16.4	Autonomous	2	60	April 2019	73.8	73.8	73.7
9	Gaztetape	19.4	Autonomous	3	60	March 2019	74.8	74.8	43.3
10	Malkorbe	30.9	Autonomous	1	60	March 2019	80.4	80.4	18.5
11	Zarautz	110.4	Non-autonomous	3	30	June 2010	76.1	76.1	70.2
12	Antilla	30.3	Autonomous	3	60	March 2019	86.5	86.5	22
13	Hondarribia	61	Autonomous	2	60	August 2018	65.5	65.5	30.2

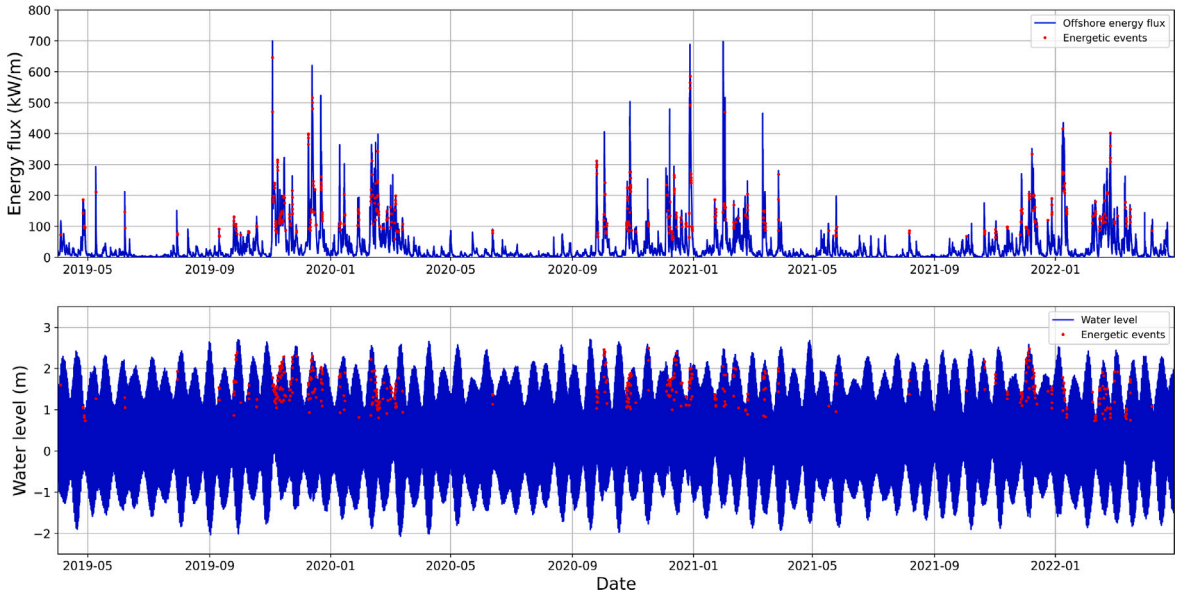

Fig. 2. Offshore energetic events during daylight hours. Top) Energy flux. Bottom) Water level (astronomical and meteorological tide) referred to the 0 of the Spanish topographic institute (NMMA IGN 2008). Red dots represent the identified energetic events during daylight hours (8 am–4 pm, UTC).

high tide (above a tide threshold, 0.73 m). In addition, the effect of the T_p is considered through the energy flux which provides a more physically relevant energetic event definition:

$$P = \frac{1}{16}\rho g {H_s}^2 C_g \quad (1)$$

where C_g represents the wave group velocity, H_s the significant wave height, ρ the density of the ocean's water (1025 kg/m^3) and g the gravitational acceleration (9.81 m/s^2).

In Fig. 2, the evolution of the energy flux (top) and water level (bottom) is shown along the study period (Apr-2019, Apr-2022). A total of 1178 energetic events were identified corresponding to 86 storms (wave heights above a threshold value during a significant time, see Oke (2002), de Santiago et al. (2017), Morton et al. (1997) for storm definition). Considering just daylight hours (8 am–4 pm, UTC), therefore, overlapping with the videometry network data, 422 energetic events are present (red dots), corresponding to 29 storms. They are representative of moderately energetic events with low return periods as the maximum extreme values (700 kW/m) are close to the average of the highest energy flux computed over the entire data set (1979–2022).

3. Methodology

3.1. Nearshore wave conditions

The propagation of wave data from deep waters up to the breaking depth at each beach is performed using the Snell's law under linear theory to characterize the nearshore hydrodynamic conditions. Snell's formulation was selected due to the fast computation, which facilitates its application within a coastal management tool.

It was compared against the data collected from a wave pressure sensor deployed at 17 m water deep at the beach of Zarautz (Fig. 1, 11) for 2 months (since the 23rd of February until the 30th of April of 2021). During the data acquisition period, variable wave conditions are captured. Applying Snell's rule, the RMSE is around 0.3 m, 2 s and 13° for H_s, T_p and Dir, respectively and the correlation coefficients ranges from 0.74 to 0.96. Both the BIAS and the SI are generally low. This is consistent with the errors obtained in previous experiments carried out at the Basque Coast with the monochromatic version of REF/DIF, a parabolic refraction–diffraction model (Kirby et al., 1994) in de Santiago et al. (2017). This shows that a simpler approach can provide adequate results.

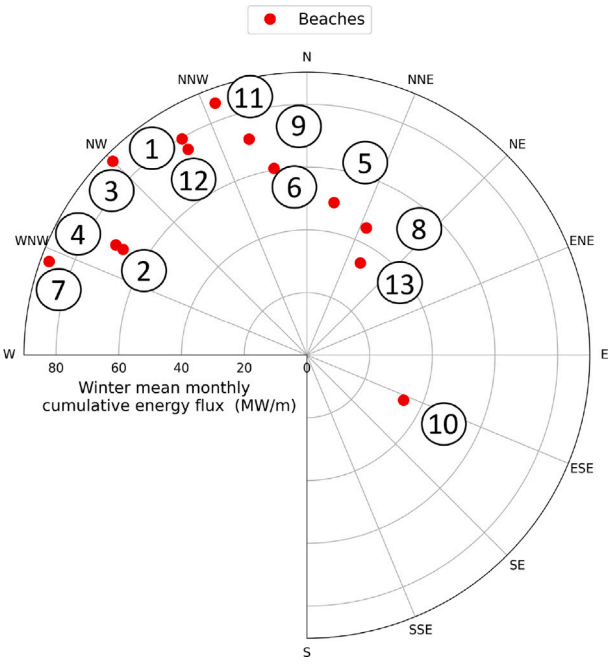

Fig. 3. Winter mean monthly cumulative energy flux (WMMCEF) at the Basque beaches. The numbers refer to the beaches shown in Fig. 1.

The comparison between winter mean monthly cumulative energy flux (WMMCEF) and beach orientation (Table 1) is shown in Fig. 3. The nearshore wave characteristics vary considerably between sites. Maximum (minimum) WMMCEF of 87.5 MW/m (34 MW/m) is registered in Arriatera (Malkorbe). While beaches facing W to N directions present WMMCEF values ranging between 60.5–87.5 MW/m, the beaches facing N to SE present WMMCEF values fluctuating between 34–49.4 MW/m, 2 times lower. This is attributed to the virtually unidirectional (fourth quadrant) wave incidence at the Basque Coast. East-facing beaches (5, 8, 10, 13; Fig. 1) are protected from energetic events and show lower wave heights than west-facing beaches (1, 2, 3, 4, 6, 7, 9, 11, 12; Fig. 1). For instance, in Fig. 4, the comparison of the energy flux between Arriatera (west-facing) and Malkorbe (east-facing) is shown along the study period, highlighting their differences in terms of magnitude.

3.2. Storm impact determination

The storm impact scale presented by de Santiago et al. (2017) (modified from Sallenger (2000)) is used to define the potential impact of storms. For that, Snap, Timex and Timestack images, (Table 2) are used. The analysis of the images is performed visually on specific areas of the image (specific beach sectors, Fig. 1, below, dark lines). Those sectors are considered the most vulnerable of the beach due to the presence of facilities, such as, restaurants and roads. If the facilities cover multiple sectors, the zone with the lowest height of the crest of the first line of defence is selected. The storm impact regime (SIR) is composed by: (i) swash regime, which represents an event where the wave runup is confined to the beach foreshore (Fig. 5; a, b), (ii) collision regime, which represents an event where the wave runup exceeds the threshold of the dune/seawall toe height and is referred to the wave structure interaction (Fig. 5; c, d) and (iii) overwash/overtopping regime, which represents an event where the wave runup overtops the dune/seawall crest height (Fig. 5; e, f, g). The obtained SIR is assumed to be representative of the impact regime over 1 h (de Santiago et al., 2017).

In order to carry out the analysis, the hydrodynamic conditions must meet the previously defined thresholds (wave height and water level) during daylight hours and the 13 videometry systems must also be simultaneously active. This leads to a total of 31 energetic events corresponding to 9 storms during the period 2019–2022 to carry out the study (Fig. 6).

3.3. Pre-storm geomorphological parameters determination

The dry beach width (DBW), the dune/seawall toe (TH) and crest heights (CH) are chosen as pre-storm geomorphological indicators (Fig. 7 and Table 3), since previous studies suggest that all, or at least one of them, might influence the storm impact intensity (de Santiago et al., 2018; Morichon et al., 2018; Silveira et al., 2016; Pesantez et al., 2022; Almeida et al., 2012).

The DBW is determined manually through orthorectified Timex images. For that, according to Wright (1980) and Díez et al. (2017), the distance between the dune/seawall toe (last line of defence) and the shoreline position at mean high tide elevation (1.8 m referred to the 0 of the Spanish topographic Institute NMMA IGN 2008) was measured at specific beach profiles, (Fig. 1, below, dark lines) defined in Section 3.2.

Due to the tidal pattern (semidiurnal) at the study site, a maximum DBW sampling resolution of 14 days can be achieved (the mean high tide level is only present during 2 spring cycles per month). Considering that the mean high tide level has to coincide with daylight hours, low Hs and fair-weather conditions (not common during high energetic conditions) to allow a good image digitalisation, the 14-day sampling resolution of the DBW is, in most cases, not viable. Hence, a 30-day data sampling resolution is chosen, as it allows to adequately cover the ranges of variability of beaches at a seasonal scale (Splinter et al., 2013; de Santiago et al., 2013). This approach allowed the sampling of around 400 DBW values during the study period.

Fig. 8 represents the schematisation of the selected DBW value for each of “n” identified energetic events during a month. Each energetic event will be related to the linearly interpolated value of DBW representative of the precedent conditions of the beach. This approach has been derived to account for the variability of abrupt erosion processes during storms (hours), while the slower recovery processes (months) (Montreuil et al., 2020; Fellowes et al., 2022; Miller and Dean, 2004; Biausque and Senechal, 2019; de Santiago et al., 2013) are covered by with a monthly sampling resolution (Splinter et al., 2013).

The TH and CH were obtained at specific beach sectors, (Fig. 1, below, dark lines) defined in Section 3.2 through airborne LiDAR (Light Detection and Ranging) surveys from 2017 and assumed as constant during the study period.

In Table 3 the mean values of DBW are represented for each beach, fluctuating between 5 and 229 m, with deviations between 3 and 9 m and minimums and maximums between 0 and 240 m respectively. TH, values are spanning from 3 to 7.5 m. The CH has values ranging between 4 and 16 m.

4. Results

4.1. Storm impact analysis

The storm impact is assessed at each beach as a function of the SIR (Fig. 5). In Fig. 9, it is shown that the storm impact is variable along the Basque beaches. Swash, collision and overtopping regimes are observed. However, just the former is present along all the beaches. On 6 out of 13 beaches the storm impact is fully dominated by a single regime (swash). On other 6 beaches, the storm impact is composed of two regimes (swash and collision). Specifically, the collision regime is dominant in 2 beaches (67.7-96.7%) and present in 4 beaches (3.3–6.4%). Only, one beach (Zarautz) experienced the three types of storm impact regime during the study period.

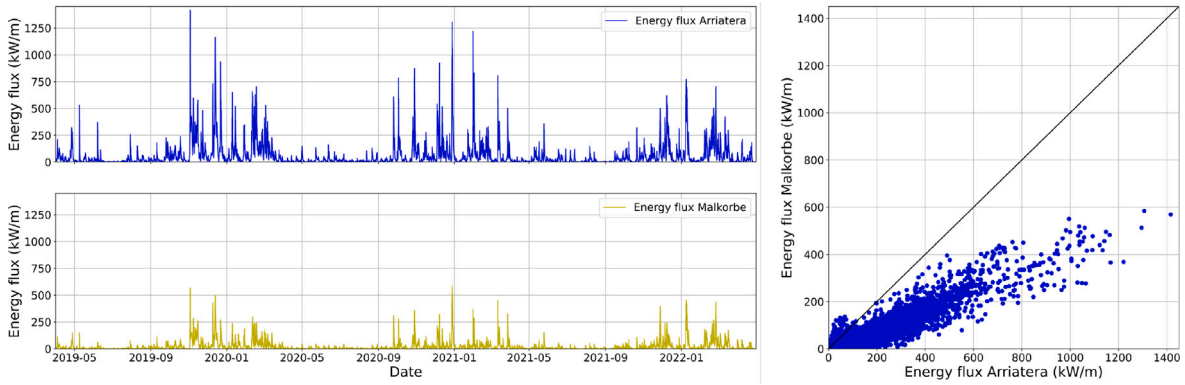

Fig. 4. Nearshore energy flux comparison. Blue) Energy flux at Arriatera. Yellow) Energy flux at Malkorbe.

Table 3
Geomorphological parameters. Dry beach width (DBW), dune/seawall toe (TH) and crest height (CH) (referred to the 0 of the Spanish topographic Institute NMMA IGN 2008). The numbers (N°) refer to the beaches shown in Fig. 1.

N°	Beach	Dry beach width (m)				Dune/Seawall toe height (m)	Dune/Seawall crest height (m)
		Average	Desv	Min	Max		
1	Muskiz	52	8	25	70	Dune: 6,5	9
2	Arrigunaga	69	3	58	74	Dune: 7,5	16
3	Arriatera	56	9	38	83	Seawall: 5	6,2
4	Saturraran	53	3	48	60	None: 5	5
5	Ondarbeltz	94	7	77	122	Dune: 5	5
6	Deba	73	6	53	85	Seawall: 4,8	5
7	Itzurun	23	5	13	36	Seawall: 3,5	7
8	Santiago	188	5	168	197	Dune: 5	5
9	Gaztetape	5	7	0	23	Seawall: 3	9
10	Malkorbe	74	7	52	88	Seawall: 4	4
11	Zarautz	10	4	1	20	Seawall: 3,5	4,5
12	Antilla	90	5	78	102	Seawall: 5	6,5
13	Hondarribia	229	4	216	240	Seawall: 4	6,5

4.2. Nearshore hydrodynamics influence on the storm impact regimes

The SIR occurrence is compared against the nearshore energy flux and water level in Fig. 10. The swash regime (Fig. 10, (a)) represents the 80.1% of the recorded cases. It mostly occurs (53.3%) for energy flux and water levels ranging between 0–200 kW/m and 0.73–1.93 m, respectively. The collision regime covers the 19.7% of the data (Fig. 10, (b)) and occurs with the energy flux and water levels ranging between 50–650 kW/m and 0.73–2.53 m, respectively. A single overtopping regime was recorded throughout the series (Fig. 10, (c)) coinciding with energy flux and water levels of 375 kW/m and 2.43 m, respectively. This energetic event occurs the 3rd of October of 2020 at 4 pm (UTC). It has the highest WL value of all the studied energetic events. There is a subtle relationship between the hydrodynamic conditions and the SIR level as the impact intensity increases with increasing wave energy flux and water levels. The swash regime is more frequent when low energy wave conditions coincide with low water levels. This pattern is more scattered when applied to the collision regime, where no clear association is found. The overtopping event coincides with energetic wave conditions and high-water level.

4.3. Influence of pre-storm geomorphological parameters on the storm impact regime

The relation between the SIR and pre-storm geomorphological parameters is shown in Fig. 11. There seems to be a correlation between the SIR, DBW, TH and CH. Swash fully dominates at locations with wide DBW values above 75 m or large TH values above 7 m while partially dominates at regions with DBW between 30 m and 75 m or TH between 3 m and 7 m. When the DBW is narrow below 30 m or the TH is low below 4 m the collision regime becomes dominant. Only when the DBW is shorter than 15 m, the TH is lower than 4 m and the CH is of 4.5 m the overtopping regime occurs. Therefore, while the DBW and TH have an influence filtering all the different regimes, the CH only filters the overtopping regime.

4.4. Common beach behaviours

In Fig. 12, the relation between the SIR frequency of occurrence (bars, left axis), DBW (boxplots, right axis blue), TH (points, right axis yellow) and CH (triangles, right axis yellow) values is shown for each beach. Three beach groups can be distinguished: Group 1 (G1)) Beaches dominated by the collision regime. These are characterised by low DBW (< 30 m) and TH (< 3.5 m) values. Group 2 (G2)) Beaches dominated by the swash regime but with combined regimes (swash and collision). These are characterised by moderate DBW (40 m–75 m) and relatively high TH (4 m–6.5 m) values. Group 3 (G3)) Beaches fully dominated by the swash regime. These beaches have relatively high DBW (> 50 m) and TH (4 m–7.5 m) values.

G1 is composed of 3 beaches, from highest to lowest values of DBW and TH increasing the storm impact intensity Itzurun, Zarautz and Gaztetape. G2 is composed of 4 beaches, from highest to lowest values of DBW and from lowest to highest values of TH, Malkorbe, Arriatera, Saturraran and Muskiz. G3 is composed of 6 beaches, describing the same sequence as G2, Hondarribia, Santiago, Antilla, Ondarbeltz, Deba and Arrigunaga. Within the beaches of the G1 the storm impact intensity is buffered as the DBW and TH increases. The inverse correlation between the pre-storm geomorphological parameters (DBW and TH) shown in G2 and G3 leads to a uniform frequency of occurrence of the SIR within groups. From beaches with the highest values of TH and

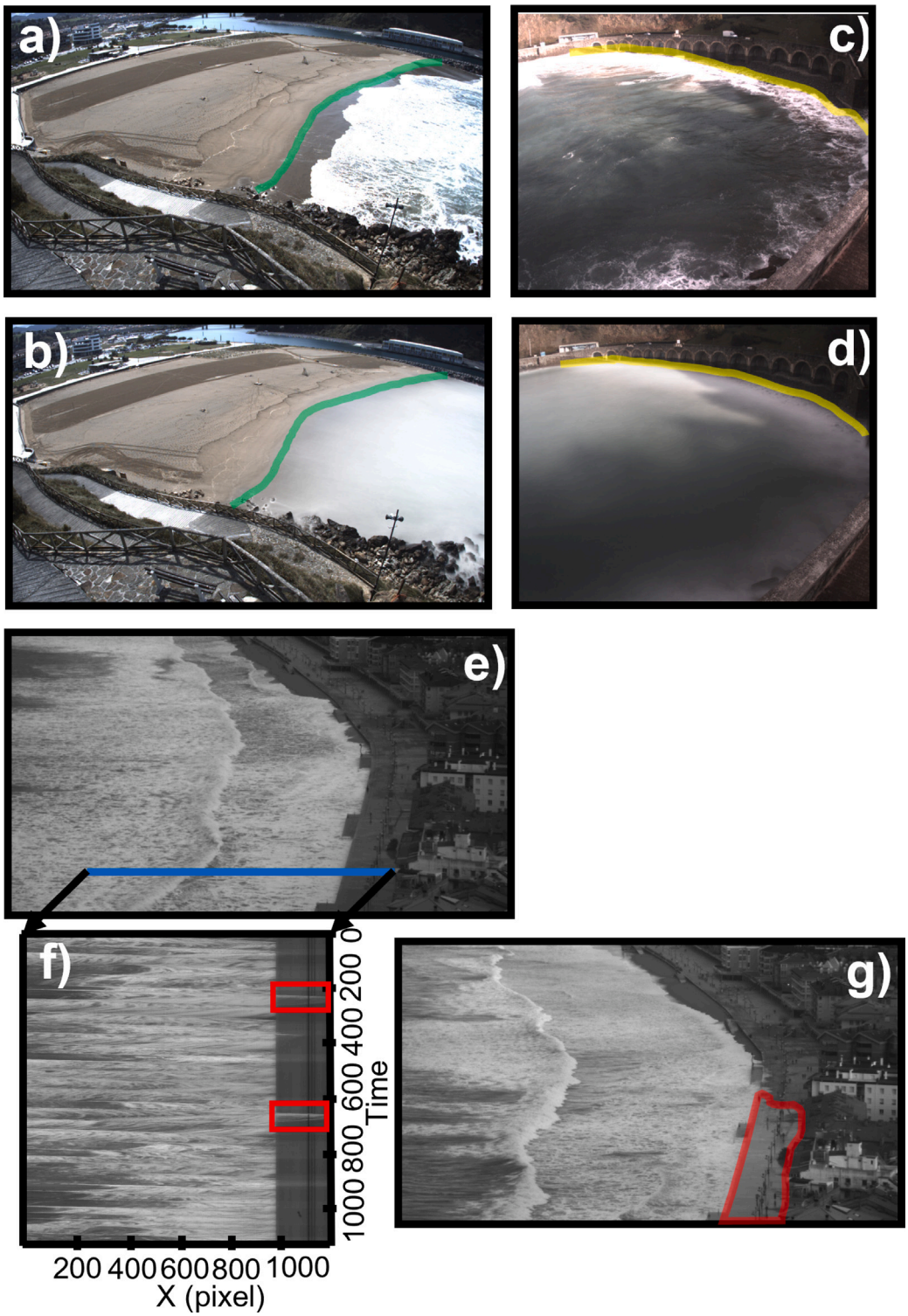

Fig. 5. Identified storm impact regime (SIR) from Snap, Timex and Timestack images. a,b) Antilla beach, Swash SIR (green) in Snap and Timex images respectively (25/09/2019; 12:00). c,d) Gaztetape beach, Collision SIR (yellow) in Snap and Timex images respectively (2/10/2020; 15:00). e,f,g) Zarautz beach (Timestack profile represented in blue), Overtopping SIR (red) in Timestack (f) and Snap (e,g) images (14/12/2020; 15:00–16:00).

lowest values of DBW (G2: Muskiz, G3: Arrigunaga) to beaches with the highest values of DBW and lowest values of TH (G2 :Malkorbe, G3: Hondarribia). This highlights the compensatory effects between the DBW and the TH values have an influence in the storm impact intensity.

5. Discussion

In the present work, storm impact through the well-known and widely-applied storm impact scale (de Santiago et al., 2017 adapted from Sallenger, 2000) is studied on the Basque beaches through an

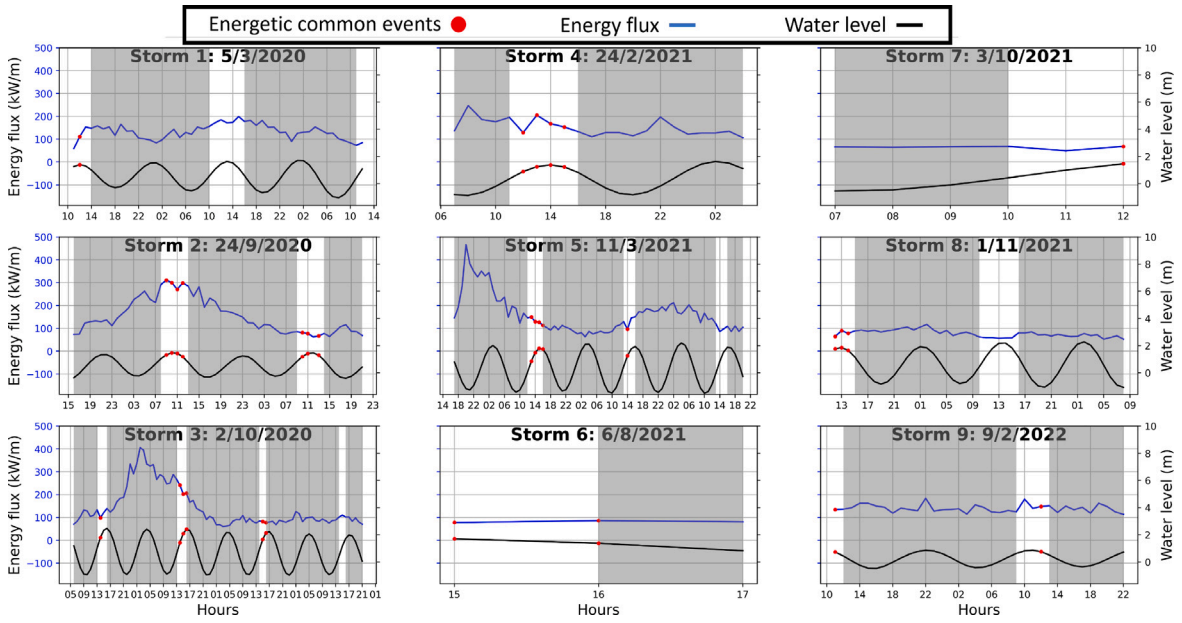

Fig. 6. Series of available energetic events during the storms under study. Blue lines: Offshore energy flux evolution during each storm. Black lines: Water level evolution during each storm. Red dots: energetic events captured by the 13 stations. Gray shadow: non-available images related to low light images (night) and water levels below the fixed threshold.

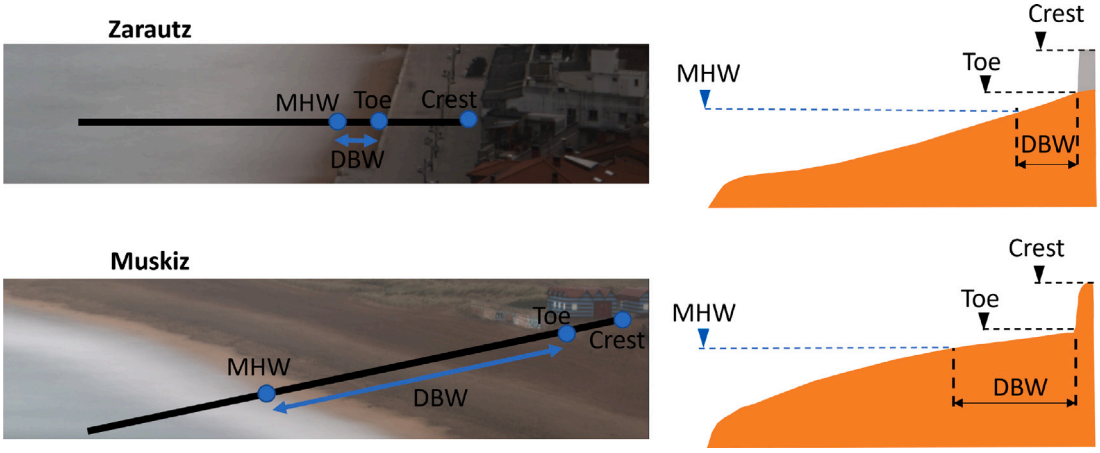

Fig. 7. Pre-storm geomorphological parameters representation. Left: Timex images of Zarautz (above) and Muskiz (below) the 14th of November of 2021 (mean high tide). Right: Representative profile of a seawall (above) and dunes (below). The dark line represents the location of the analysed profile.

extensive video monitoring network. In addition, its relation with the nearshore hydrodynamics and pre-storm geomorphological characteristics is analysed.

5.1. Video-monitoring systems advantages and limitations

Coastal videometry is widely used for multiple applications (Splinter et al., 2018a; Andriolo et al., 2019; Santos et al., 2020; Liria et al., 2021; Epelde et al., 2021; Addona et al., 2022). The Basque videometry network is currently used for; occupation density analysis (Epelde et al., 2021), rip currents detection and forecast (Liria et al., 2021) and shoreline evolution analysis (de Santiago et al., 2021; Chust et al., 2022) which makes this tool multi-functional. However, this paper is the first attempt to investigate storm impact through storm impact regime data (which is rare at the present, Callens et al., 2021) at regional scale.

Conducting a field survey to address the storm impact regime and pre-storm geomorphological characteristics in a single site is a challenging task due to adverse meteomarine conditions and high costs (Addona et al., 2022). Therefore, carry them in multiple sites (high spatial resolution), repeatedly (high temporal resolution) during a large period is virtually impossible. In that sense, the use of coastal videometry compared to field surveys is a cost-effective solution. Even if coastal videometry stations need to be maintained during their life cycle (around 10 years), these costs are low.

Nevertheless, coastal videometry has certain limitations. Just 31 events were captured by all the videometry stations simultaneously in contrast to the 422 available events. While both autonomous and non-autonomous videometry stations experienced camera malfunctions related to adverse weather conditions (*e.g.* camera's point of view shift) or damages in the hardware, they were more frequent in autonomous stations due to battery issues (low charge) that lead to connection failures and reduced data acquisition periods during cloudy weather (usually coinciding with storm events). These systems, although more experimental, are easy to implement at any location, and require a limited infrastructure, leading to lower costs and less administrative procedures. Their performance is expected to improve in the near future as technological development progress. For instance, it could be

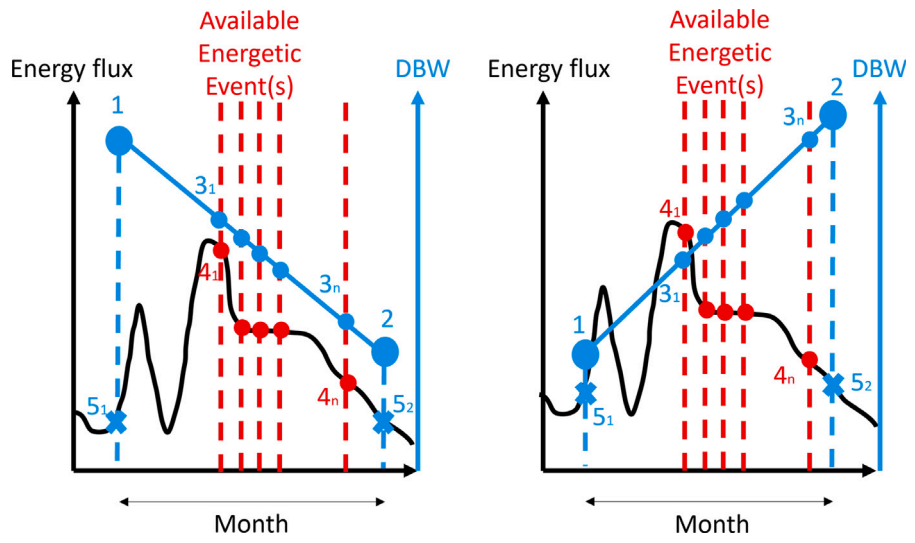

Fig. 8. Schematisation of the selected dry beach width (DBW) value for each of "n" identified energetic events during a month. Left: Example of DBW decrease between the monthly data sampling. Right: Example of DBW increase between the monthly data sampling. (1,2) DBW monthly sampling values. (3) DBW interpolated values for each of "n" energetic events date representative of the beach precedent conditions. (4) Energy flux value of each of "n" energetic events. (5) Low energetic conditions during DBW monthly sampling values.

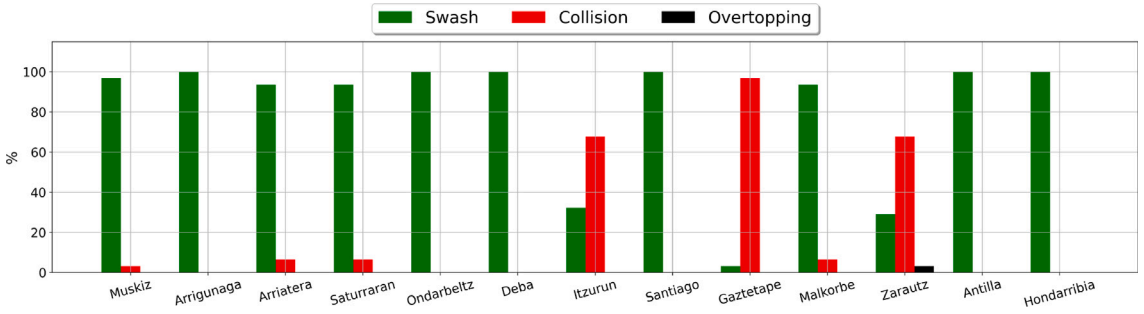

Fig. 9. SIR frequency of occurrence. Green: Swash, Red: Collision, Black: Overtopping. Beaches are ordered from west to east.

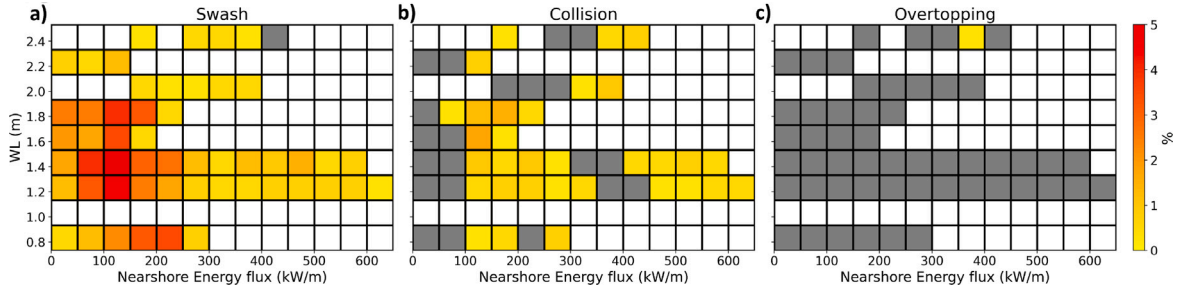

Fig. 10. Occurrence of SIR for different nearshore energy flux and water levels. a) Swash. b) Collision. c) Overtopping. White bins: non existing data in the studied database. Shaded bins: existing data in the studied database but belonging to other SIR. Colorbar: SIR percentage of occurrence along all the analysed energetic events.

improved by using more efficient solar panels/batteries or through the optimisation of image recording methods.

The presented limitations highlight the need of continuous maintenance activities of the videometry systems to ensure a proper data acquisition. In addition, to increase the amount of data, high temporal resolution (at least 30 min) and the inclusion of NIR cameras (which can be used at low light conditions) at the most exposed areas, would be desirable.

5.2. Storm impact assessment

Previous studies mention that the storm impact intensity is highly controlled by the tide filtering effect, increasing during high water levels (de Santiago et al., 2017; Stein and Siegle, 2020). Moreover, the storm impact intensity is expected to increase with the storm magnitude (de Santiago et al., 2017; Stein and Siegle, 2020). On the contrary, the filtering effect of the tide and the influence of the storm magnitude is not clear in the present study. This is because the analysed nearshore energy flux and water level ranges correspond to already filtered values, thus, their effect in the storm impact intensity is not that relevant in the analysis. However, it is not excluded to find patterns associating the storm impact intensity with the nearshore hydrodynamic conditions when extending the range to low energy conditions or even to more severe conditions. In contrast, we find that storm impacts are influenced by the beach pre-storm geomorphological parameters, as wider DBW and/or higher TH the storm impact intensity is buffered. This might be

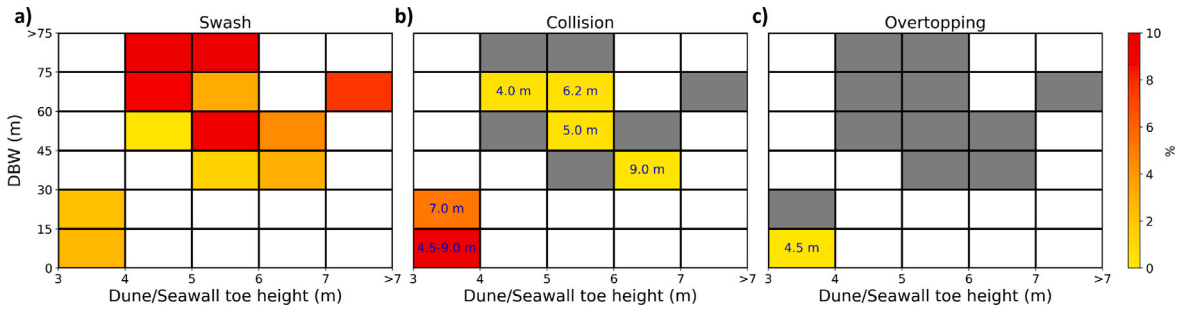

Fig. 11. Occurrence of SIR for different DBW, TH and CH. a) Swash. b) Collision. c) Overtopping. White bins: non existing data in the studied database. Shaded bins: existing data in the studied database but belonging to other SIR. Blue numbers: CH values and ranges for each bin. Colorbar: SIR percentage of occurrence along all the analysed energetic events.

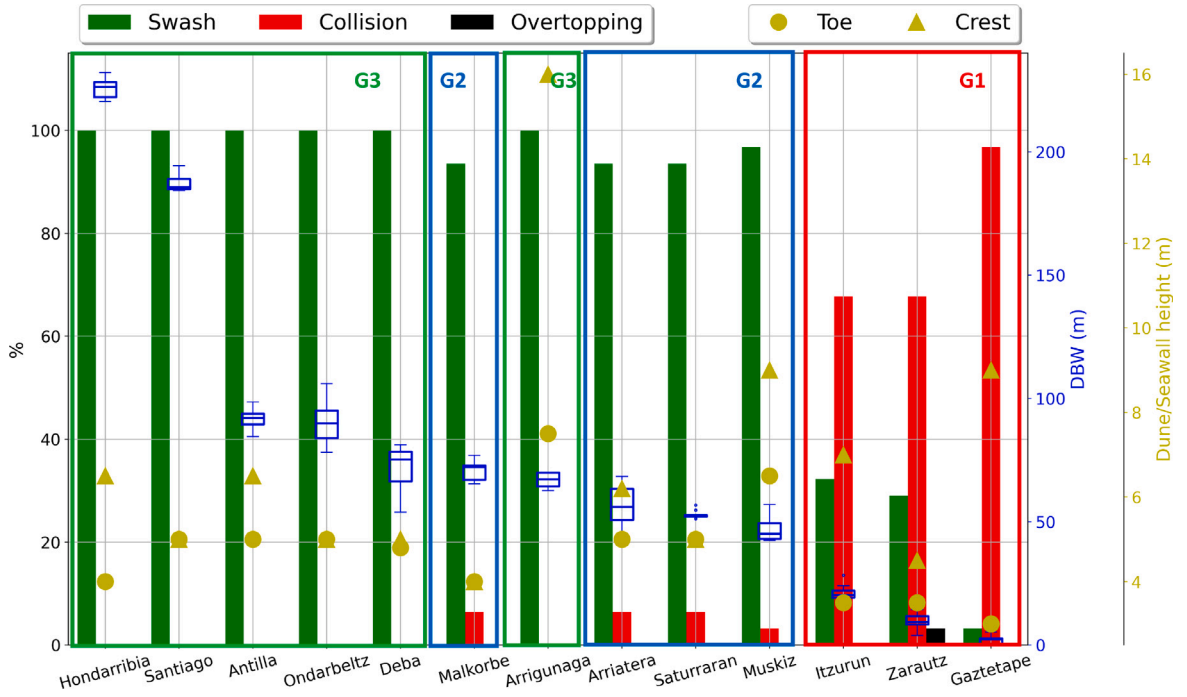

Fig. 12. SIR, DBW, TH and CH representation for the 31 energetic events at each beach with beach groups defined. Left axis: SIR frequency of occurrence. Right axis (blue): Boxplots of DBW. Right axis (yellow): TH (circle) and CH (triangle). Beaches are ordered according to their DBW (descending order).

directly related to the natural barrier that represents the subaerial part of the beach, as wider and higher is, higher is the degree of protection. This also highlights the relation between the DBW and the TH. Beaches with a small (large) beach width are usually related to low (high) toe elevation (Díez et al., 2018). These findings are in line with Carapuço et al. (2016), de Santiago et al. (2018), Morichon et al. (2018), Silveira et al. (2016), Pesantez et al. (2022) where the influence of pre-storm geomorphological parameters on the storm impact regime is noted. However, exceptions as the mutual compensation of both parameters (DBW and TH) related to the storm impact intensity were found. Very high values of DBW or TH seems to compensate low values of TH or DBW respectively, reducing the storm impact intensity (Hondarribia and Arrigunaga). The overtopping event registered in the data series shows the relevance of the CH as higher values made collision prevail while low values derive into overtopping (Zarautz). Other indicators, (such as the beach slope; Carapuço et al., 2016; Nguyen et al., 2016; Benavente et al., 2006; Medellín et al., 2021; Stein and Siegle, 2020; Almeida et al., 2012 or sandbars configuration; Medellín et al., 2021) might have small nuances in the obtained results, but it is not assessed in the present study as the full variability of the storm impact intensity along beaches is explained through the subaerial parameters.

It is worth to highlight that a uniform value of the TH may be enough at beaches where swash regime is dominant regime, however, at beaches with a dominant collision regime, the evolution of TH should be considered as it was done with the DBW.

5.3. Recommendations for further research and application for coastal management

This study highlights that the Basque regional coastal videometry network could provide valuable information to decision makers and other stakeholders. This information is useful to identify the most exposed beaches to storm impact and their drivers along the Basque coast. Indeed, to buffer the storm impact intensity, the DBW and the TH should be increased in the most exposed beaches (G1) and at least conserved in the less exposed ones (G2, G3).

The application of the methodology presented in this study to other sites with regional scale coastal videometry networks would allow to contrast the results and extrapolate the methodology to different hydro-morphological conditions. Different examples of globally and regionally extended technologies are found in the literature. The ORASIS Coastal Video Monitoring System (Vousdoukas et al., 2011) covers 10 beaches along the world from which 6 are located in Greece. The Cam-era

computer-controlled cameras (Coco et al., 2004) that covers 5 beaches in New Zealand. The Argus video monitoring system (Holman et al., 1993; Aarninkhof and Holman, 1999) that covers around 30 beaches along the world from which 7 are located in the east and west coasts of United States, 4 in the east coast of Australia, 3 in Netherlands, 2 in the UK and 3 in Spain. The COSMOS Coastal Monitoring System (Taborda and Silva, 2012) that covers 5 beaches in Portugal. Other remote sensing techniques, such as, CoastSnap (Harley et al., 2019) (https://www.https://www.coastsnap.com) and satellite imagery could be an alternative to a regional coastal videometry network, as they provide a wide spatial coverage of images. Both techniques allow to collect the geomorphological data from images but, are not designed to extract storm impact data so far. Those techniques would be useful to characterize storm impact through the collected geomorphological data in sites with similar hydro-morphological characteristics to the Basque Coast.

The interpretation and transference of the developed information should be supported by the interaction between stakeholders and the scientific community. This interaction should be reciprocal. In this sense, stakeholders are advised to coordinate the work of multidisciplinary experts (*e.g.* scientists, coastal engineers, urbanistic technicians) and to take part during the research process. In addition, scientific community delegates could be included in the development of the policies and regulations.

6. Summary and conclusions

The present study assesses the variability of the storm impact through the well-known and widely-applied storm impact scale (de Santiago et al., 2017 adapted from Sallenger, 2000), identifies the relation between storm impact, nearshore hydrodynamics and pre-storm geomorphology and finds common beach behaviours at a regional scale using an extensive video monitoring network (Liria et al., 2021; Epelde et al., 2021) operating along the Basque Coast, highlighting the potential of a spatially wide coastal videometry network for coastal management purposes.

Storm impacts are variable along the Basque beaches, being the swash regime dominant for the studied events. The influence of nearshore hydrodynamic conditions on the SIR (storm impact regime) do not follow a clear pattern. However, an adequate relation was found between storm impacts and two pre-storm geomorphological parameters of beaches. The results show that as higher is the DBW (dry beach width) and/or the TH (dune/seawall toe height) lower is the storm impact intensity (swash) and inversely (collision). This is directly related to the natural barrier that represents the subaerial part of the beach, as wider and higher is, higher will be the degree of protection.

Based on these findings, the beaches of the study site were described as a function of storm impacts and pre-storm geomorphological parameters as: Group 1) Beaches dominated by the collision regime that present low values of DBW and TH, specifically, DBW lower than 30 m and TH below 3.5 m. Group 2) Beaches dominated by the swash with few collision events that present moderate values of DBW and relatively high values of TH, specifically, DBW values between 40 and 75 m and TH between 4 and 6.5 m. Group 3) Beaches fully dominated by the swash regime that present relatively high values of DBW and so the TH, specifically, DBW values above 50 m and TH between 4 and 7.5 m.

This study will help to support coastal management strategies identifying the most exposed beaches that would require special attention and in some cases priority investment. In addition, the drivers identification will benefit stakeholders to support coastal management strategies, through uniform adaptation measures along different beach groups. Therefore, the need of an adequate maintenance for stakeholders of video-monitoring stations is highlighted.

CRediT authorship contribution statement

Aritz Abalia: Conceptualisation, Data curation, Methodology, Writing – original draft, Writing – review & editing. **Iñaki de Santiago:** Conceptualisation, Formal analysis, Methodology, Writing – review & editing. **Pedro Liria:** Conceptualisation, Data curation, Formal analysis, Writing – review & editing. **Roland Garnier:** Conceptualisation, Formal analysis, Writing – review & editing. **Irati Epelde:** Data curation, Formal analysis, Writing – review & editing. **Asier Nieto:** Data curation, Formal analysis, Writing – review & editing. **Denis Morichon:** Conceptualisation, Formal analysis, Methodology, Writing – review & editing.

Declaration of competing interest

The authors declare that they have no known competing financial interests or personal relationships that could have appeared to influence the work reported in this paper.

Data availability

The authors do not have permission to share data.

Acknowledgements

This study has been supported by the KOSTARISK joint laboratory (funded by AZTI, UPPA and RPT), the Urban Klima 2050 – LIFE 18 IPC 000001 project (funded by the European Union's LIFE programme), and the Regions4Climate project (Horizon Europe, DOI: 10.3030/101093873). Roland Garnier acknowledges funding from the Provincial Council of Gipuzkoa through the Fellows Gipuzkoa Programme (Ref: 2022-FELL-000004-01). We thank the Puertos del Estado for wave and tidal gauge measurements. This paper is the contribution number 1220 from AZTI, Marine Research, Basque Research and Technology Alliance (BRTA).

References

Aarninkhof, S., Holman, R., 1999. Monitoring the nearshore with video. Backscatter 10 (2), 8–11.

Addona, F., Sistilli, F., Romagnoli, C., Cantelli, L., Liserra, T., Archetti, R., 2022. Use of a raspberry-pi video camera for coastal flooding vulnerability assessment: The case of Riccione (Italy). Water 14 (7), 999.

Almeida, L.P., Vousdoukas, M.V., Ferreira, Ó., Rodrigues, B.a., Matias, a., 2012. Thresholds for storm impacts on an exposed sandy coastal area in southern Portugal. Geomorphology 143–144, 3–12.

Andriolo, U., Sánchez-García, E., Taborda, R., 2019. Operational use of surfcam online streaming images for coastal morphodynamic studies. Remote Sens. 11 (1), 1–21.

Benavente, J., Del Río, L., Gracia, F.J., Martínez-del Pozo, J.A., 2006. Coastal flooding hazard related to storms and coastal evolution in Valdelagrana spit (Cadiz Bay Natural Park, SW Spain). Cont. Shelf Res. 26 (9), 1061–1076.

Biausque, M., Senechal, N., 2019. Seasonal morphological response of an open sandy beach to winter wave conditions: The example of Biscarrosse beach, SW France. Geomorphology 332, 157–169.

Callens, A., Morichon, D., Liquet, B., 2022. Bayesian networks to predict storm impact using data from both monitoring networks and statistical learning methods. Nat. Hazards (0123456789).

Callens, A., Morichon, D., Liria, P., Epelde, I., Liquet, B., 2021. Automatic creation of storm impact database based on video monitoring and convolutional neural networks. Remote Sens. 13 (10), 1–20.

Carapuço, M.M., Taborda, R., Silveira, T.M., Psuty, N.P., Andrade, C., Freitas, M.C., 2016. Coastal geoindicators: Towards the establishment of a common framework for sandy coastal environments. Earth-Sci. Rev. 154, 183–190.

Chust, G., González, M., Fontán, A., Revilla, M., Alvarez, P., Santos, M., Cotano, U., Chifflet, M., Borja, A., Muxika, I., Sagarminaga, Y., Caballero, A., de Santiago, I., Epelde, I., Liria, P., Ibaibarriaga, L., Garnier, R., Franco, J., Villarino, E., Irigoien, X., Fernandes-Salvador, J.A., Uriarte, A., Esteban, X., Orue-Echevarria, D., Figueira, T., Uriarte, A., 2022. Climate regime shifts and biodiversity redistribution in the Bay of Biscay. Sci. Total Environ. 803.

Coco, G., Bryan, K., Payne, G., 2004. The next era for cam-era. Coast. News 26, 22–24.

Cohn, N., Brodie, K., Conery, I., Spore, N., 2022. Alongshore variable accretional and erosional coastal foredune dynamics at event to interannual timescales. Earth Space Sci. 9 (12), e2022EA002447.

Cueto Fonseca, J., Otero Díaz, L., Ospino Ortiz, S., Torres-Freyermuth, A., 2021. The role of morphodynamics in predicting coastal flooding from storms on a dissipative microtidal beach with SLR conditions: Cartagena de Indias (Colombia). Nat. Hazards Earth Syst. Sci. Discuss. (July), 1–25.

Daly, C.J.J., Bryan, K.R., Roelvink, J.A., Klein, A.H.F., Hebbeln, D., Winter, C., Klein, H.F., Hebbeln, D., Winter, C., 2011. Morphodynamics of embayed beaches: the effect of wave conditions. J. Coast. Res. (64), 1003–1007.

de Santiago, I., Camus, P., González, M., Liria, P., Epelde, I., Chust, G., del Campo, A., Uriarte, A., 2021. Impact of climate change on beach erosion in the Basque Coast (NE Spain). Coast. Eng. 167, 103916.

de Santiago, I., Morichon, D., Abadie, S., Castelle, B., Liria, P., Epelde, I., 2013. Video monitoring nearshore sandbar morphodynamics on a partially engineered embayed beach. J. Coast. Res. 65, 458–463.

de Santiago, I., Morichon, D., Abadie, S., Reniers, A.J.H.M., Liria, P., 2017. A comparative study of models to predict storm impact on beaches. Nat. Hazards 87, 843–865.

de Santiago, I., Morichon, D., Arnoux, F., Delpey, M., Epelde, I., 2018. Risk mapping assessment by means of probabilistic storm scenarios in a partially engineered beach: Anglet, France. J. Coast. Res. 85 (10085), 796–800.

Díez, J., Cánovas, V., Uriarte, A., Medina, R., 2017. Characterization of the dry beach profile: A morphological approach. J. Coast. Res. 33 (6), 1292–1304.

Díez, J., Cohn, N., Kaminsky, G.M., Medina, R., Ruggiero, P., 2018. Spatial and temporal variability of dissipative dry beach profiles in the Pacific Northwest, U.S.A.. J. Coast. Res. 34 (3), 510–523.

Epelde, I., Liria, P., de Santiago, I., Garnier, R., Uriarte, A., Picón, A., Galdrán, A., Arteche, J.A., Lago, A., Corera, Z., et al., 2021. Beach carrying capacity management under Covid-19 era on the Basque Coast by means of automated coastal videometry. Ocean & Coastal Management 208, 105588.

Fellowes, T.E., Vila-Concejo, A., Gallop, S.L., 2019. Morphometric classification of swell-dominated embayed beaches. Mar. Geol. 411, 78–87.

Fellowes, T.E., Vila-Concejo, A., Gallop, S.L., Harley, M.D., Short, A.D., 2022. Wave shadow zones as a primary control of storm erosion and recovery on embayed beaches. Geomorphology 399, 108072.

González, M., Uriarte, A., Fontán, A., Mader, J., Gyssels, P., 2004. Marine dynamics. Oceanogr. Mar. Environ. Basque Ctry. 70, 133–157.

Harley, M.D., Kinsela, M.A., Sánchez-García, E., Vos, K., 2019. Shoreline change mapping using crowd-sourced smartphone images. Coast. Eng. 150, 175–189.

Holland, K.T., Holman, R.A., Lippmann, T.C., Stanley, J., Plant, N., 1997. Practical use of video imagery in nearshore oceanographic field studies. IEEE J. Ocean. Eng. 22 (1), 81–91.

Holman, R.A., Sallenger, A.H., Lippmann, T.C., Haines, J.W., 1993. The application of video image processing to the study of nearshore processes. Oceanography 6 (3), 78–85.

Kirby, J.T., Dalrymple, R.A., Kaku, H., 1994. Parabolic approximations for water waves in conformal coordinate systems. Coast. Eng. 23 (3–4), 185–213.

Kroon, A., Davidson, M., Aarninkhof, S., Archetti, R., Armaroli, C., Gonzalez, M., Medri, S., Osorio, A., Aagaard, T., Holman, R., et al., 2007. Application of remote sensing video systems to coastline management problems. Coast. Eng. 54 (6–7), 493–505.

Liria, P., Chust, G., Epelde, I., Caballero, A., 2011. Extreme wave flood-risk mapping within the Basque coast. J. Coast. Res. 225–229.

Liria, P., Epelde, I., Santiago, I., Garnier, R., Abalia, A., Mader, J., 2021. Kostasystem, a coastal videometry technology: Development and applications. In: 9th EuroGOOS International Conference.

Medellín, G., Mayor, M., Appendini, C.M., Cerezo-Mota, R., Jiménez, J.A., 2021. The role of beach morphology and mid-century climate change effects on wave runup and storm impact on the Northern Yucatan Coast. J. Mar. Sci. Eng. 9 (5).

Miller, J.K., Dean, R.G., 2004. A simple new shoreline change model. Coast. Eng. 51, 531–556.

Montreuil, A.-L., Chen, M., Brand, E., Verwaest, T., Houthuys, R., 2020. Post-storm recovery assessment of urbanized versus natural sandy macro-tidal beaches and their geomorphic variability. Geomorphology 356, 107096.

Morichon, D., De Santiago, I., Delpey, M., Somdecoste, T., Callens, A., Liquet, B., Liria, P., Arnould, P., 2018. Assessment of Flooding Hazards at An Engineered Beach during Extreme Events: Biarritz, SW France. J. Coast. Res. 85 (i), 801–805.

Morton, I.D., Bowers, J., Mould, G., 1997. Estimating return period wave heights and wind speeds using a seasonal point process model. Coast. Eng. 31 (1–4), 305–326.

Mucerino, L., Albarella, M., Carpi, L., Besio, G., Benedetti, A., Corradi, N., Firpo, M., Ferrari, M., 2019. Coastal exposure assessment on Bonassola bay. Ocean & Coastal Management 167, 20–31.

Nguyen, T.T., Bonetti, J., Rogers, K., Woodroffe, C.D., 2016. Indicator-based assessment of climate-change impacts on coasts: A review of concepts, methodological approaches and vulnerability indices. Ocean & Coastal Management 123, 18–43.

Nieto, M.A., Garau, B., Balle, S., Simarro, G., Zarruk, G.A., Ortiz, A., Tintoré, J., Álvarez-Ellacuría, A., Gómez-Pujol, L., Orfila, A., 2010. An open source, low cost video-based coastal monitoring system. Earth Surf. Process. Landf. 35 (14), 1712–1719.

Oke, T.R., 2002. Boundary Layer Climates. Routledge.

Pesantez, J.E., Behr, A., Sciaudone, E., 2022. Importance of pre-storm morphological factors in determination of coastal highway vulnerability. J. Mar. Sci. Eng. 10 (8), 1158.

Roelvink, D., Reniers, A., Van Dongeren, A., De Vries, J.V.T., McCall, R., Lescinski, J., 2009. Modelling storm impacts on beaches, dunes and barrier islands. Coast. Eng. 56 (11–12), 1133–1152.

Sallenger, Jr., A.H., 2000. Storm impact scale for barrier islands. J. Coast. Res. 890–895.

Santos, C.J., Andriolo, U., Ferreira, J.C., 2020. Shoreline response to a sandy nourishment in a wave-dominated coast using video monitoring. Water (Switzerland) 12 (6), 1–15.

Silveira, T.M., Taborda, R., Carapuço, M.M., Andrade, C., Freitas, M.C., Duarte, J.F., Psuty, N.P., 2016. Assessing the extreme overwash regime along an embayed urban beach. Geomorphology 274, 64–77.

Splinter, K.D., Harley, M.D., Turner, I.L., 2018a. Remote sensing is changing our view of the coast: Insights from 40 years of monitoring at Narrabeen-Collaroy, Australias. Remote Sens. 10 (11).

Splinter, K.D., Kearney, E.T., Turner, I.L., 2018b. Drivers of alongshore variable dune erosion during a storm event: Observations and modelling. Coast. Eng. 131, 31–41.

Splinter, K.D., Turner, I.L., Davidson, M.A., 2013. How much data is enough? The importance of morphological sampling interval and duration for calibration of empirical shoreline models. Coast. Eng. 77, 14–27.

Stein, L.P., Siegle, E., 2020. Overtopping events on seawall-backed beaches: Santos Bay, SP, Brazil. Reg. Stud. Mar. Sci. 40, 101492.

Stockdon, H.F., Sallenger, A.H., Holman, R.a., Howd, P.a., 2007. A simple model for the spatially-variable coastal response to hurricanes. Mar. Geol. 238 (14), 1–20.

Stokes, K., Poate, T., Masselink, G., King, E., Saulter, A., Ely, N., 2021. Forecasting coastal overtopping at engineered and naturally defended coastlines. Coast. Eng. 164, 103827.

Taborda, R., Silva, A., 2012. COSMOS: A lightweight coastal video monitoring system. Comput. Geosci. 49, 248–255.

Toimil, A., Álvarez-Cuesta, M., Losada, I., 2023. Neglecting the effect of long-and short-term erosion can lead to spurious coastal flood risk projections and maladaptation. Coast. Eng. 179, 104248.

Tolman, H., 2016. The WAVEWATCH III development group. WAVEWATCHIII development best practices.

Vousdoukas, M.I., Ferreira, P.M., Almeida, L.P., Dodet, G., Psaros, F., Andriolo, U., Taborda, R., Silva, A.N., Ruano, A., Ferreira, Ó.M., 2011. Performance of intertidal topography video monitoring of a meso-tidal reflective beach in South Portugal. Ocean Dyn. 61, 1521–1540.

Vousdoukas, M.I., Wziatek, D., Almeida, L.P., 2012. Coastal vulnerability assessment based on video wave run-up observations at a mesotidal, steep-sloped beach. Ocean Dyn. 62, 123–137.

Wright, L., 1980. Beach cut in relation to surf zone morphodynamics. In: Coastal Engineering 1980. pp. 978–996.

Zijlema, M., Stelling, G., Smit, P., 2011. SWASH: An operational public domain code for simulating wave fields and rapidly varied flows in coastal waters. Coast. Eng. 58 (10), 992–1012.